Geometrical Simplification of Complex Kinetic Systems

Rex T. Skodje* and Michael J. Davis

Department of Chemistry, University of Colorado, Boulder, Colorado 80309 and Chemistry Division, Argonne National Laboratory, Argonne, Illinois 60439

Received: March 5, 2001; In Final Form: May 31, 2001

The use of low-dimensional manifolds to simplify the description of complicated systems of kinetics equations is investigated. Many models exhibit a generic behavior, whereby kinetic trajectories rapidly approach a surface of much lower dimension than that of the full phase space of concentrations, and subsequently show slow relaxation to equilibrium restricted to the surface. Traditional methods, such as the quasi-steady-state approximation, can be viewed as approximate schemes to construct the low dimensional manifolds. A number of techniques for the construction of low-dimensional manifolds are discussed and compared. A more general formulation of several previous methods is provided. A new technique, the global eigenvalue method, is derived. This method combines the conceptual advantages of the Maas−Pope algorithm with the accuracy of global trajectory propagation. One- and two-dimensional manifolds are constructed using the global eigenvalue method for a 38-reaction mechanism for hydrogen combustion. A new formulation of sensitivity analysis is provided which allows testing a reduced mechanism to changes in the rate constants.

I. Introduction

It is common for realistic reaction mechanisms to involve many elementary reaction steps and many distinct chemical species.[1] For example, the recent model of Chevalier et al.[2] for the ignition of heptane contains 620 chemical species and about 7000 reactions. Obviously, then, quantitative models for the kinetics of such systems become large and, sometimes, physically obscure. If a homogeneous, isothermal system consists of *N*-chemical species and *M*-elementary reactions, then its kinetics is described by *N*-ordinary differential equations (ODEs) each of which may contain up to *M* terms. Furthermore, the ODEs are generally stiff[3] because the values for the elementary rate constants are typically distributed over a wide range of magnitudes. Despite their complexity, kinetic trajectories (i.e., solutions to the kinetics equations) can often be obtained for very large models using efficient stiff solvers such as LSODE.[4] Although they are powerful tools, packages such as LSODE are not panaceas. If spatial inhomogeneity is included, e.g., in modeling flames, the simulation may still become intractable.[5] Furthermore, if the number of independent species grows too large, such as with polymerization reactions, the computation may become impossible. In a more conceptual sense, the availability of an efficient ODE solver does not provide a physical picture for the reaction even if the kinetic trajectories can be numerically generated. In practical terms, the simple agreement between numerical trajectories and experimental data is often insufficient to establish the accuracy of elementary rate constants.

For all of the reasons mentioned above, there is considerable interest in developing schemes for kinetic simplification.[6,7] The essential goal of kinetic simplification is to devise reduced mechanisms containing a smaller number of independent species that can reproduce the characteristics of the larger models. The most familiar approach employs the quasi-steady-state-approximation (QSSA) wherein the rate equations for unstable intermediates are set to zero.[1,8] Each of the resulting algebraic equations can be used to eliminate one species from the model. Although it is an inherently approximate method, the QSSA can be systematically applied and often yields good results. More recently, lumping techniques have been devised which explicitly combine elementary species concentrations into a smaller number of "lumped" concentrations.[9] The resulting reduced mechanism involves ODE's only for the lumped species. Other more formal techniques use singular perturbation theory to eliminate transient species from the mechanism that result from inherent separation of time scales.[10] One technique that has attracted considerable attention in the combustion kinetics community is the intrinsic low-dimension manifold (ILDM) method of Maas and Pope.[11,12,13,14] In the ILDM technique, a local analysis of the kinetics equations is used to identify rapidly and slowly contracting directions in the phase space of concentrations. At "long times" kinetic trajectories are observed to collapse to the vicinity of curvilinear low dimensional manifolds defined as surfaces on which the flow is oriented purely in the slow directions. The ILDM method will be discussed in more detail in section II because it serves as the starting point for our global eigenvalue method.

Recently, we have discussed geometrical approaches to kinetic simplification.[15,16] From this viewpoint, simplified models are constructed employing attracting low-dimensional manifolds (ALDM) in the phase space of concentrations. If there are N-independent chemical species, then full phase space in which kinetic trajectories can evolve is N-dimensional. Simplification occurs when, on some sufficiently long time scale, trajectories within the phase space all collapse to neighborhood of some much lower dimensional manifold that is generally curvilinear. The ALDM differs from the ILDM of Maas and Pope in that the ALDM represents the exact manifold to which propagated trajectories attract, whereas the ILDM is an approximation based on infinitesimally propagated trajectories. Thus, the ALDM is a global attractor while the ILDM is a local attractor.

10.1021/jp0108465 CCC: $20.00
Published on Web 10/23/2001

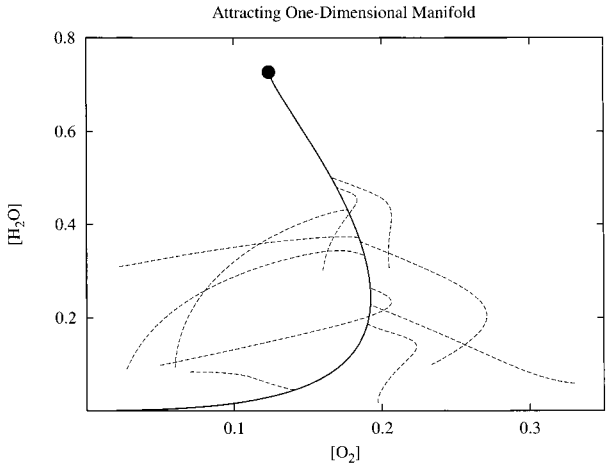

Figure 1. One-dimensional manifold for hydrogen combustion. The solid line represents the one-dimensional ALDM obtained using the global eigenvalue method. The dashed lines are randomly selected trajectories started at various initial conditions and show rapid attraction to the manifold on time scales of 10^{-3} s. The large dot is the equilibrium point. The conditions chosen for the simulation were $T = 1500$ K, $p = 0.207$ bar, $C_1 = 10^{16}/\text{cm}^3$, and $C_2 = 1.5 \times 10^{16}/\text{cm}^3$.

As an illustration, in Figure 1, we plot a one-dimensional ALDM for the problem of hydrogen combustion, which will be discussed in section III. There are eight species; thus, the phase space is nominally eight-dimensional, yet on a time scale of 0.01 s, trajectories of widely different initial conditions approach a single one-dimensional curve. Thus, to simulate the kinetics on long times, the full model may be replaced a much smaller model which only includes the manifold. Hence, in principle, at long times there is only one independent species, albeit a nonlinear function of the all the other species. In a sense, the QSSA, the ILDM, lumping, and perturbation theory all give approximations to the ALDM. In some cases, the approximation errors may be small. However, it is important to have techniques available to obtain the exact ALDM for cases when approximate methods fail.

The physical basis for kinetic simplification using ALDM is a separation of time scales that derive from intrinsically fast and slow reactions. Fast reactions give transient behavior, which we do not attempt to simplify, whereas the remaining slow processes define the asymptotic dynamics along a low dimensional manifold. From the standpoint of phase space dynamics, fast and slow kinetics processes translate into rapidly and slowly contracting directions in phase space. Along the ALDM, the trajectories evolve orthogonal to the rapidly contracting directions in a manner to be described below.

Pioneering work on the construction of ALDM has been carried out by Fraser and Roussel,[17,18,19,20] who used the term "slow manifolds". The essential observation of Fraser and Roussel was that the ALDM could be viewed as an attracting fixed point of a functional mapping. Thus, an initial guess for the ALDM could be iteratively improved. Fraser and Roussel applied the mapping technique to several low-dimensional problems in enzyme kinetics using computer algebra to iterate the formal kinetics equations. In previous work, we modified the format of the iteration to represent species concentrations on numerical grids, which allows the technique to be applied to much larger mechanisms. Furthermore, it was found that numerical instabilities in the iteration could be quenched by breaking each functional iteration into a number of partial iterations that were implemented as a numerical integration. Further details will be provided in section III.

In this article, we shall discuss several techniques for the construction of the ALDM. Some of the techniques discussed have been presented previously and are reproduced in a somewhat more general context. The main focus here will be the derivation of a new method, the global eigenvalue method, which combines the intuitive appeal of the MP(Maas−Pope)-algorithm with the accuracy of exact trajectory based methods. The method is applied to a 38-reaction mechanism for hydrogen combustion. One and two-dimensional ALDMs are constructed and discussed. The use of the ALDM for sensitivity analysis will be presented.

II. Methods for Constructing Manifolds

A. Kinetics on Manifolds. When a kinetic mechanism is simplified using a low-dimensional manifold, it is necessary to re-express the kinetic equations in terms of a coordinate parametrization of the manifold. In the simplest cases, this might involve merely selecting a subset of the initial concentrations to serve as the independent variables. In general, however, the manifold can be folded which leads to a multivalued function in this representation. Therefore, as a prelude to the discussion of the techniques for manifold construction, we discuss how the reduced mechanism can be expressed in terms of a general single valued parametrization of the manifold.

Consider a homogeneous kinetic system consisting of n-chemical species, $[A_1,...,A_n]$, which are described by a vector of positive concentrations, $\mathbf{y}(t) = [y_1(t),...,y_n(t)]$. The kinetic scheme is composed of M-elementary reactions of arbitrary order. Thus, the concentrations usually solve the equations

$$\frac{d\mathbf{y}}{dt} = \mathbf{F}(\mathbf{y}) \tag{2.1}$$

where

$$F_i(\mathbf{y}) = \sum_{j=1}^{M} \upsilon_{i,j} R_j \tag{2.2}$$

and

$$R_i = k_i(T) \cdot y_{i_1}^{\ p_1} \cdots y_{i_n}^{\ p_n} \tag{2.3}$$

The coefficients $\upsilon_{i,j}$ are chosen consistent with the molecularities of the reaction steps. In general, the dimensionality of the phase space of concentrations can, and should, be reduced by using the N_C constants of motion consistent with the kinetic scheme. For a closed system, these constants would include those for conservation of mass of each element present but also may include other constants associated with symmetries in the kinetics equations (2.1). Thus, for a given choice of constants, the system is $N = n - N_C$ dimensional. By convention, we will eliminate the last N_C species from the concentration vector, $\boldsymbol{y}$, and the rates, $\boldsymbol{F}$, which shall henceforth be considered as N-dimensional vectors.

We begin with a discussion of one-dimensional manifolds, M_1. The manifold is a continuous curve, $[Y_1(s),...,Y_N(s)]$ in the N-dimensional space, which is parametrized by s, some smooth function of $\boldsymbol{y}$. Thus

$$Y_i = Y_i(s) \tag{2.4}$$

and

$$s = s(\mathbf{y}) \tag{2.5}$$

In the simplest case, s may be taken as one of the species concentrations. The kinetics equations can be written as

$$\frac{dy_i}{ds} = \frac{F_i(\mathbf{y})}{ds/dt} \tag{2.6}$$

where ds/dt can be replaced by

$$\frac{ds}{dt} = \sum_{i=1}^{N} \frac{\partial s}{\partial y_i} \cdot F_i(\mathbf{y}(s)) \tag{2.7}$$

The only restriction on M_1 at this point is that it follows the orbit of an actual kinetic trajectory. Equation 2.7, applied to the "special" orbit $\boldsymbol{Y}(s)$, effectively provides a one-dimensional reduced mechanism for the kinetics described by (2.1).

An m-dimensional manifold, M_m, can be parametrized by m-functions

$$s_j = s_j(\mathbf{y}) \tag{2.8}$$

which leads to the first-order partial differential equation

$$\sum_{j=1}^{m} \frac{\partial y_i}{\partial s_j} \cdot \frac{ds_j}{dt} = F_i \tag{2.9}$$

where

$$\frac{ds_j}{dt} = \sum_{i=1}^{N} \frac{\partial s_j}{\partial y_i} \cdot F_i(\mathbf{y}(\mathbf{s})) \tag{2.10}$$

Again, we assume here only that the manifold is constructed from exact solutions to the kinetic equations. The m-equations in (2.10) provide an m-dimensional reduced model.

Implicit in all low-dimensional manifold methods is the need to construct an explicit representation of the manifold. In most cases, one is given a finite number of points on the manifold, e.g., as values of kinetic trajectories at discrete time steps, $\boldsymbol{y}(t_k)$. The manifold can be continuously represented using polynomial or spline interpolation with these data. A manifold of fixed dimension must be constrained to be smooth, i.e., differentiable, in keeping with the physical interpretation of eq 2.1. The most difficult matter is the need to construct a globally single valued parametrization of the manifold. For a local patch of the manifold, it is always possible to construct a chart that parametrizes an m-dimensional manifold using points in $\boldsymbol{R}^m$.[21] However, the use of a number of distinct charts is unwieldy as a practical matter, and a global coordinate system is desirable. If subset of m-concentrations for which the manifold is single valued cannot be found, it is possible that m-linear combinations of concentrations can be used. A given choice can be tested against the requirement that all m-partial derivatives remain bounded on the manifold.

For a one-dimensional manifold, a convenient parametrization is simply the propagation time along the orbit. Given a trajectory, $\boldsymbol{y}(t)$, which follows the manifold, $\boldsymbol{Y}(s)$, for $t>0$ we have

$$s = \int_0^t dt = \int_{y_0}^{\mathbf{y}} \frac{\mathbf{F} \cdot d\mathbf{y}}{\mathbf{F} \cdot \mathbf{F}} \tag{2.11}$$

Because the manifold orbit generally slows as it progresses along the manifold, the logarithm of the propagation time tends to provide a more satisfactory parameter. Higher dimensional manifolds require more effort to reconstruct from trajectory data because families of orbits must be combined. Time may be used as one parameter, but trajectory indices must be also employed.

To achieve an accurate simplification of a kinetic model, it is necessary to locate the ALDM to which kinetic trajectories are attracted at sufficiently long times. In the following sections, we shall present several strategies for constructing these manifolds. For completeness, we begin with a discussion of known methods that are local in phase space. That is, methods that involve an analysis of the kinetics equations at single points. Except for linear systems, such methods are approximate although they can be quite accurate. Our main focus, however, shall be on global methods that (implicitly or explicitly) involve trajectories propagated for finite times. In principle, global methods can be converged by testing the attractivity of the manifolds for increasing time intervals.

B. Local Approximations for ALDM. As noted above, the physical basis for the simplification of kinetic systems is a separation of time scales. For local methods, such as the QSSA and MP algorithms, fast and slow processes are inferred by examining the kinetics equations at isolated points in phase space. In the QSSA approximation, the fast processes are assumed to dominantly involve highly reactive intermediate species. By setting the corresponding rate equations to zero, i.e., $0 = F_i(\boldsymbol{y})$, one is effectively identifying the manifold where the rapid transient has decayed.

The MP-approximation represents a significant advance over the QSSA-method in both accuracy and generality. The fast and slow local directions in phase space can be found without the need to arbitrarily identify certain species as being highly reactive intermediates. Indeed, the eliminated species can be combinations of all the species and nonlinear functions in phase space.

The simplest way to derive the MP-approximation is to consider the evolution of the kinetic trajectories for very short time interval, Δt. For Δt small, we can solve the kinetics equation by first-order Taylor expansion. Consider the trajectory flow in the vicinity of a central trajectory, $\boldsymbol{y}_0(t)$. Trajectories neighboring $\boldsymbol{y}_0(t)$ in phase space are described by the displacement vector

$$\delta\mathbf{y}(t) = \mathbf{y}(t) - \boldsymbol{y}_0(t) \tag{2.12}$$

To first-order in the displacement, we may approximate eq 2.1 as

$$\frac{d(\delta\mathbf{y})}{dt} = \mathbf{J} \bullet \delta\mathbf{y} \tag{2.13}$$

where the Jacobian matrix, $\boldsymbol{J}$, is

$$J_{i,j} = \frac{\partial F_i}{\partial y_j}\Big|_{\mathbf{y}=\mathbf{y}_0} \tag{2.14}$$

For very short time intervals, Δt, we may approximate $\boldsymbol{J}$ as a constant, which then renders eq 2.12 into the form of a linear system with constant coefficients. Choosing an eigenvector basis, $[\mathbf{z}_1,...\mathbf{z}_N]$ to express $\delta\boldsymbol{y}$, the time scales can be identified through the familiar expression

$$\delta\mathbf{y} = \sum_{j=1}^{N} c_j \mathbf{z}_j e^{\lambda_j \Delta t} \tag{2.15}$$

where

$$\mathbf{J} \cdot \mathbf{z}_j = \lambda_j \mathbf{z}_j \tag{2.16}$$

The eigenvectors of the most negative $Re(\lambda_i)$ correspond to the most strongly contracting directions. The eigenvectors of the least negative $Re(\lambda_i)$ define the slowest contracting directions.

In the Maas−Pope algorithm, the attracting m-dimensional manifold (IDLM) is defined as the points in phase space where the $N-m$ fastest eigenvectors have zero-projection along the kinetic flow, i.e.

$$\langle z_j|F\rangle = 0 \; j = m+1,...,N \tag{2.17}$$

Equation 2.17 defines the sense in which the ILDM is orthogonal to the directions of transient decay and, thus, represents pure asymptotic motion. In general, the loci of points defining the manifold are determined numerically using, e.g., Newton's method to locate phase space points where eq 2.17 is satisfied. The method is expected to be most accurate for large separation of time scale. For a linear system, eq 2.14 can be extended to arbitrary large Δt and thus the MP-method is exact for such systems. Errors in the MP-method are found[15,22] to be largest where the curvature of the manifold is highest. We find that the MP-method is most stable when the eigenspace is represented using vectors obtained using Gramm-Schmidt orthogonalization. We should also note that the numerical implementation of the method becomes problematic when the eigenvalues cross as one proceeds along the manifold.

C. Global Methods. The local methods for the determination of ALDM's have often proven satisfactory for kinetic simplification. However, such methods are inherently approximate and occasionally pathological. Global methods can, in principle, converge to the exact ALDM and are generally more desirable. At the minimum, global methods are useful to give error estimates for local methods. Here, we discuss several strategies for the determination of globally attractive manifolds.

1. Trajectory Methods. As seen in Figure 1, the attracting manifold, M_1, describes the long time evolution of every trajectory, but it is shadowed for longer distances by those trajectories started further from the equilibrium point. The intuitive basis of our predictor-corrector method, described in ref 15, is to start a trajectory "very" far away from equilibrium, which thus is attracted to and becomes indistinguishable from the manifold for the physically relevant regions of phase space. In general, to obtain the manifold over the full range, it is necessary to start the trajectories in regions where some of the concentrations are negative, i.e., unphysical regions of phase space. This can create problems because there is no guarantee that unphysical trajectories will approach equilibrium. Thus, in the predictor−corrector method, it was necessary to carefully extend the starting point of the trajectory backward in a progressive fashion that ensured the trajectory approached equilibrium and was physically reasonable.

Another trajectory-based approach discussed in ref 15 is the "saddlepoint" method. Many systems possess saddlepoints in phase space, $\boldsymbol{y}_s$, which are stationary points, i.e., $\boldsymbol{F}(\boldsymbol{y}_s) = 0$, having at least one positive $\mathrm{Re}(\lambda_i)$ and, thus, at least one repelling direction in phase space. The saddlepoints invariably occur in the unphysical region of phase space, yet can be crucial in defining global structures in phase space such as the boundaries of basins of attraction. The manifold emanating from the most unstable direction of the saddle can be propagated into the physical region of phase space and ultimately to the equilibrium point to yield the global attracting one-dimensional manifold. In favorable cases, families of orbits may be propagated to construct higher-dimensional manifolds.

2. Modified Fraser Algorithm. As mentioned in the Introduction, Fraser and Roussel have suggested an iterative scheme to generate the ALDM.[17,18,19,20] In this method, time is eliminated from the rate equations to give orbit equations in phase space. Thus, for a one-dimensional manifold parametrized for simplicity by the concentration y_1 as the independent variable we have, by dividing pairs of equations in (2.1)

$$\frac{\mathrm{d}y_i/\mathrm{d}t}{\mathrm{d}y_1/\mathrm{d}t} = \frac{\mathrm{d}y_i}{\mathrm{d}y_1} = \frac{F_i}{F_1} \equiv g_i(\mathbf{y},y_1) \tag{2.18}$$

The manifold is thus parametrized by y_1 and time is eliminated. The key observation of Fraser and Roussel was that eq 2.18 can be used to set up an iterative functional mapping for which the ALDM is a fixed point. We imagine an initial guess for the slow manifold written as an *N-1* dimensional vector

$$\mathbf{y}^0(y_1) = [y_2{}^0(y_1),... ,y_N{}^0(y_1)]^T \tag{2.19}$$

A mapping is defined as

$$\frac{\mathrm{d}\mathbf{y}^n}{\mathrm{d}y_1} = \mathbf{g}(\mathbf{y}^{n+1},y_1) \tag{2.20}$$

that can be numerically inverted to provide the explicit iteration

$$\mathbf{y}^{n+1} = \mathbf{H}\left(\frac{\mathrm{d}\mathbf{y}^n}{\mathrm{d}y_1};y_1\right) \tag{2.21}$$

where $\mathbf{H}$ is the inverse function of $\boldsymbol{g}$. Provided that the initial guess is reasonable, iteration of eq 2.21 was found to approach a slow manifold.

Previously,[15] we have generalized and modified the Fraser−Roussel method for application to larger kinetic systems. In the original formulation, the manifold was represented through analytic functions and the iteration was accomplished with a symbolic manipulator such as MAPLE. We found a more facile representation was to adopt a spatial grid for the independent variable, y_1, upon which the dependent concentrations were numerically expressed. The derivatives, $\mathrm{d}\mathbf{y}^n/\mathrm{d}y_1$, were then evaluated with finite difference formulas and the iteration was accomplished numerically at each grid point. As noted earlier, however, the mapping is only asymptotically convergent, so that after enough iterations the manifold eventually "buckles" and diverges. The convergence of the iteration, eq 2.21, was stabilized by effectively breaking up each iteration into a sequence of fractional iterations which could ultimately be written as a differential equation in a continuous iteration variable, τ

$$\frac{\mathrm{d}\mathbf{y}}{\mathrm{d}\tau} = \mathbf{H} - \mathbf{y} \tag{2.22}$$

It was found[15] that the explicit root search involved in constructing $\mathbf{H}$ could be circumvented by employing the equally accurate first-order expression

$$\frac{\mathrm{d}\mathbf{y}}{\mathrm{d}\tau} = -\,\mathbf{g}\cdot\left[\frac{\mathrm{d}\mathbf{g}}{\mathrm{d}\mathbf{y}'}\right]^{-1} \tag{2.23}$$

obtained by expansion of eq 2.22 in the change in $\boldsymbol{y}$. In eq 2.23 $\boldsymbol{y}'$ is $\mathrm{d}\boldsymbol{y}/\mathrm{d}y_1$.

Higher dimensional manifolds may also be obtained using the functional mapping technique.[19] Consider the general case where an m-dimensional manifold parametrized by the functions

s_j. Combining eqs 2.9 and 2.10, we obtain the functional mapping

$$\sum_{j=1}^{m} \frac{\partial y_i^n}{\partial s_j} \cdot \sum_{k=1}^{N} \frac{\partial s_j}{\partial y_k^{n+1}} \cdot F_k(\mathbf{y}^{n+1}) = F_i(\mathbf{y}^{n+1}) \qquad (2.24)$$

Because in this construction, $\partial y_i^n/\partial s_j$ is known while $\boldsymbol{y}^{n+1}$ is unknown, we may invert eq 2.22 to obtain the explicit functional mapping

$$\mathbf{y}^{n+1} = \mathbf{H}\left(\frac{\mathrm{d}\mathbf{y}^n}{\mathrm{d}s_1},\ldots,\frac{\mathrm{d}\mathbf{y}^n}{\mathrm{d}s_m};s_1(\mathbf{y}^n),\ldots,s_m(\mathbf{y}^n)\right)$$

which then can be applied at every grid point. As before, each iteration can be broken into a set of integration steps to stabilize the algorithm,

$$\frac{\mathrm{d}\mathbf{y}}{\mathrm{d}\tau} = \mathbf{H} - \mathbf{y}$$

3. The Global Eigenvalue Method. A method that combines some of the advantages of the MP-method with accuracy of the trajectory-based techniques is the global eigenvalue method that is presented here for the first time. Recall that the MP-method could be formulated as a search for the most attracting directions of the local dynamics, i.e., for time propagations that are infinitesimal. In the present method, we reformulate this approach assuming arbitrary finite time propagation. Consider the trajectory dynamics near to a center trajectory, $\boldsymbol{y}_0(t)$. Thus, we have

$$\frac{\mathrm{d}\mathbf{y}(t)}{\mathrm{d}t} = \mathbf{F}(\mathbf{y}) \qquad (2.25)$$

where

$$\mathbf{y}(t) = \boldsymbol{y}_0(t) + \delta\mathbf{y}(t) \qquad (2.26)$$

The dynamics of the perturbation, $\delta\boldsymbol{y}$, satisfy

$$\frac{\mathrm{d}(\delta\mathbf{y}(t))}{\mathrm{d}t} = \mathbf{J}(\boldsymbol{y}_0) \cdot \delta\mathbf{y}(t) \qquad (2.27)$$

which we recall was the starting point for the MP-method. The Jacobian matrix, defined by eq 2.14, is evaluated on the center trajectory and thus does not depend on the dependent variables $\delta\mathbf{y}(t)$. Unlike the MP-method, we do not restrict time intervals to be small, so $\boldsymbol{J}$ is time-dependent through its dependence on $\boldsymbol{y}_0(t)$. Therefore, a formal solution to the initial value problem (2.27) can be written as

$$\delta\mathbf{y}(t) = \begin{bmatrix} \frac{\partial y_1^0(t)}{\partial y_1^0(0)} & \cdots & \frac{\partial y_N^0(t)}{\partial y_N^0(0)} \\ \vdots & \ddots & \cdots \\ \frac{\partial y_1^0(t)}{\partial y_1^0(0)} & \cdots & \frac{\partial y_N^0(t)}{\partial y_N^0(0)} \end{bmatrix} \bullet \delta\mathbf{y}(0) \equiv \mathbf{M}(t) \cdot \delta\mathbf{y}(0) \qquad (2.28)$$

where $y_j^0(t)$ are the components of the center trajectory. The linear propagator matrix, **M**, is familiar from dynamical systems theory[23] and is sometimes referred to as the Mondronomy matrix. An eigenvector analysis of the **M**-matrix defines the fast and slow contracting directions of the flow. We write

$$\mathbf{M}(t) \bullet \mathbf{\Lambda}_i = \Gamma_i \mathbf{\Lambda}_i \qquad (2.29)$$

where the eigenvalues, Γ_i, and the eigenvectors, $\mathbf{\Lambda}_i$, will generally depend on time. An attracting m-dimensional manifold will be defined by the orthogonality of the flow to the $N-m$ fastest eigenvectors

$$\langle \Lambda_j | \mathbf{F} \rangle = 0 \; j = 1,\ldots,N-m \qquad (2.30)$$

In eq 2.30, the inner product is taken between the left-eigenvector of **M** and the flow vector **F** eq 2.30 is combined with a Newton−Raphson search over the initial conditions $\boldsymbol{y}_0$ to locate the points on M_m. Clearly, the global eigenvalue method becomes equivalent to the MP-algorithm when t is infinitesimally small. For finite t, the method converges to the globally accurate ALDM. In practice, to compute **M**, it is necessary to compute N-satellite trajectories that are slightly displaced from $\boldsymbol{y}_0$.

As a practical matter, we require a value for propagation time, t. This quantity should properly be regarded as a convergence parameter. Thus, there will exist a T such that when $|t| > |T|$ the manifold point is converged to some accuracy ϵ. Furthermore, there is no reason t cannot be chosen to be negative provided that eq 2.30 is applied to the largest $\mathrm{Re}(\Gamma_i)$ eigenvectors. In fact, the reverse propagation of trajectories often provides the most robust convergence of the method. Of course since the backward integration of the central trajectory is unstable, $-t$ should not be set too large.

An approximate analysis that is often accurate represents the linearized propagator $\mathbf{M}(t)$ with

$$\mathbf{M}(t) \approx \mathrm{e}^{\mathbf{A}(t)} \qquad (2.31)$$

where

$$\mathbf{A}(t) = \int_0^t \mathbf{J}(t')\mathrm{d}t' \qquad (2.32)$$

In that case, the eigenvalue analysis of **M** is equivalent to that of ***A***, which is simpler to calculate. If the kinetics equations involve only involve reaction of second order or lower, then it becomes quite simple to calculate the **A**-matrix. For such systems, each element of ***J*** is a linear function of the concentrations, so

$$A_{i,j}(t) = \int_0^t \frac{\partial F_i(y_0(t'))}{\partial y_{0,j}(t')}\mathrm{d}t' = \int_0^t (\sum_k a_{i,j,k} y_{0,k}(t') + b_{i,j})\mathrm{d}t' \qquad (2.33)$$

Thus, to compute **A** for second-order systems requires only the integration of the N-concentrations along the trajectory. Higher order approximations to **M**, obtained from the Magnus expansion[24] or the Dyson time-ordered product[25] may prove useful in some cases.

To illustrate the convergence of the method, we apply the global eigenvalue method to a simple two-dimensional model problem where the exact ALDM is analytically known.[15] The kinetics equations are given by

$$\frac{\mathrm{d}x}{\mathrm{d}t} = -x \qquad (2.34)$$

$$\frac{\mathrm{d}y}{\mathrm{d}t} = -\gamma y + \frac{(\gamma-1)x + \gamma x^2}{(1+x)^2} \qquad (2.35)$$

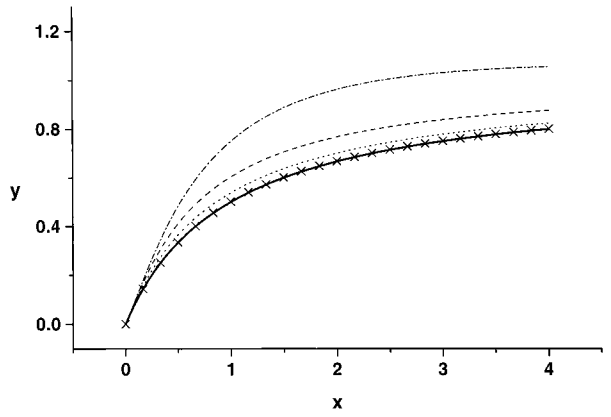

Figure 2. One-dimensional manifolds for the model problem. The solid line is the exact manifold, $y = x/(1 + x)$. The dot−dashed line is the MP-approximation. The dotted line is the $t = -1$ global eigenvalue result, while the symbols are for $t = -5$. The dash curve is the approximate result using eq 2.31 with $t = -5$.

where $\gamma > 1$. These differential equations can be solved analytically to yield

$$x(t) = x_0 e^{-t} \tag{2.36}$$

$$y(t) = \left(y_0 - \frac{x_0}{1 + x_0}\right)e^{-\gamma t} + \frac{x_0 e^{-t}}{1 + x_0 e^{-t}} \tag{2.37}$$

It is clear that the transient term, which contains the factor $e^{-\gamma t}$, goes to zero on the curve

$$y = \frac{x}{1 + x} \tag{2.38}$$

which therefore defines the one-dimensional ALDM. The linearized propagator is found directly from eqs 2.36 and 2.37

$$\mathbf{M}(0,t) = \begin{bmatrix} e^{-t} & 0 \\ \dfrac{e^{-t}}{(1 + x_0 e^{-t})^2} - \dfrac{e^{-\gamma t}}{(1 + x_0)^2} & e^{-\gamma t} \end{bmatrix} \tag{2.39}$$

The eigenvalues are $e^{-\gamma t}$ and e^{-t} the corresponding left-eigenvectors are

$$\Lambda_1{}^L = \left[\frac{e^{-t}}{(1 + x_0 e^{-t})^2} - \frac{e^{-\gamma t}}{(1 + x_0)^2}, e^{-\gamma t} - e^{-t}\right] \tag{2.40}$$

$$\Lambda_2{}^L = [1,0] \tag{2.41}$$

For negative t, the most unstable direction is defined by eq 2.40. The manifold equation $\langle \mathbf{\Lambda}_1^L | \mathbf{F} \rangle = 0$ yields

$$y = \frac{x}{1 + x} + \frac{e^{-t}}{\gamma(e^{-t} - e^{-\gamma t})}\left(\frac{x}{(1 + x e^{-t})^2} - \frac{x}{(1 + x)^2}\right) \tag{2.42}$$

The deviation from the exact manifold is seen to scale to zero with the ratio of eigenvalues, i.e., $e^{(\gamma-1)t}$.

In Figure 2, we plot the manifolds obtained for the relatively nonstiff case of $\gamma = 2$. The exact manifold is shown with a solid line. The application of eq 2.30 for infinitesimal times, which is equivalent to the MP-algorithm, gives a crude approximation to the manifold. The $t = -1$ application corrects part of the error, whereas $t = -5$ gives essentially the exact manifold. Plotted with a dashed line is the approximate expression eq 2.31 for $t = -5$. Although not perfect, this result represents a substantial improvement over the local approximation.

TABLE 1:

1	$O_2 + H \rightarrow O + OH$
2	$O + OH \rightarrow O_2 + H$
3	$O + H_2 \rightarrow H + OH$
4	$H + OH \rightarrow H_2 + O$
5	$H_2 + OH \rightarrow H + H_2O$
6	$H + H_2O \rightarrow H_2 + OH$
7	$OH + OH \rightarrow O + H_2O$
8	$O + H_2O \rightarrow OH + OH$
9	$H + H + M \rightarrow H_2 + M$
10	$H + OH + M \rightarrow H_2O + M$
11	$O + O + M \rightarrow O_2 + M$
12	$O_2 + H + M \rightarrow HO_2 + M$
13	$H + HO_2 \rightarrow OH + OH$
14	$OH + OH \rightarrow H + HO_2$
15	$H + HO_2 \rightarrow O_2 + + H_2$
16	$O_2 + H_2 \rightarrow H + HO_2$
17	$H + HO_2 \rightarrow O + H_2O$
18	$O + H_2O \rightarrow H + HO_2$
19	$O + HO_2 \rightarrow O_2 + OH$
20	$O_2 + OH \rightarrow O + HO_2$
21	$OH + HO_2 \rightarrow O_2 + H_2O$
22	$O_2 + H_2O \rightarrow OH + HO_2$
23	$HO_2 + HO_2 \rightarrow O_2 + H_2O_2$
24	$OH + OH + M \rightarrow H_2O_2 + M$
25	$H + H_2O_2 \rightarrow H_2 + HO_2$
26	$H_2 + HO_2 \rightarrow H + H_2O_2$
27	$H + H_2O_2 \rightarrow OH + H_2O$
28	$OH + H_2O \rightarrow H + H_2O_2$
29	$O + H_2O_2 \rightarrow OH + HO_2$
30	$OH + HO_2 \rightarrow O + H_2O_2$
31	$OH + H_2O_2 \rightarrow H_2O + HO_2$
32	$H_2O + HO_2 \rightarrow OH + H_2O_2$
33	$O_2 + H_2O_2 \rightarrow HO_2 + HO_2$
34	$H_2 \rightarrow H + H$
35	$H_2O \rightarrow H + OH$
36	$O_2 \rightarrow O + O$
37	$HO_2 \rightarrow O_2 + H$
38	$H_2O_2 \rightarrow OH + OH$

III. Applications

As an application of the ALDM concept, we consider the isothermal combustion of hydrogen. We adopt a model consisting of 38 elementary reactions, listed in Table 1, and 8 chemical species: H_2, O_2, H, O, OH, OOH, HOOH, and H_2O. The reaction was studied in the temperature range of 1500−4000 K, for concentrations 10^{16}−10^{17} molecule/cm^3, and in the presence of an inert buffer gas at pressures of 0.01−1 bar. The rate constants were the same as those used in ref 11, with one additional reaction added.[15] There are two exact constants of motion in this system, C_1 and C_2, which are the total oxygen-atom and hydrogen-atom concentrations, respectively. As we shall see, there is an additional quantity that is approximately conserved on certain time scales, the total concentration of molecules.

Some trajectories for $T = 1500$ K are plotted on a log/log scale in Figure 3. It is seen that there are at least three distinct time scales at work. At very short times, $< 10^{-6}$ sec, the concentrations vary independently. This is an initiation phase of the combustion. Then comes a stable region lasting between 10^{-6}−10^{-3} sec. During this interval, we see from the lower

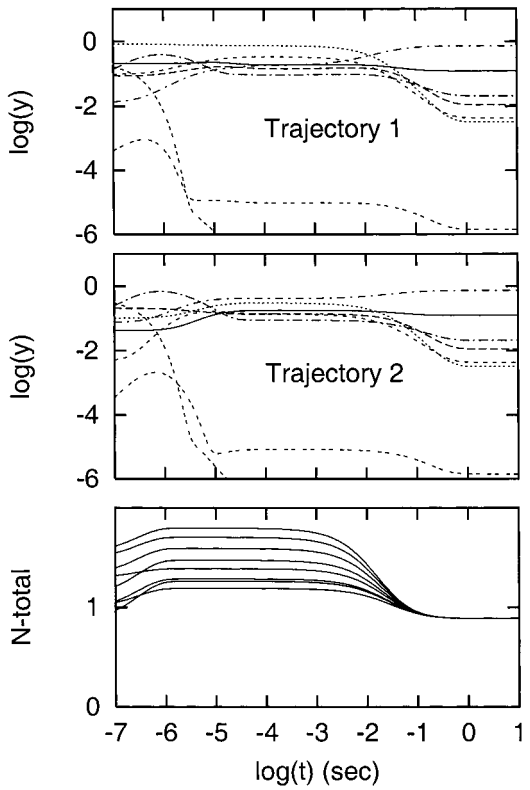

Figure 3. Logarithmic plot of the trajectories shown in Figure 1. In the first two panels, the concentrations of the eight species is plotted for two trajectories. The total total concentration, N, is plotted vs log(t) in the lower panel. The approximate conservation of N at intermediate times is clearly apparent from the plot.

panel of Figure 3 that the total concentration, N, is roughly constant, where

$$N = \sum_i y_i \tag{3.1}$$

During this time interval, the kinetics is dominated by the chain propagating steps of the mechanism. On a long time scale, $t > 10^{-3}$ sec, the value of N changes and the system eventually relaxes to equilibrium as the termination steps become important. In terms of attracting manifolds, therefore, early times $<10^{-6}$ sec are transients during which no low dimensional manifold attracts the orbits. During the intermediate times, $10^{-6}-10^{-3}$ sec, a two-dimensional manifold exists for which the total concentration is an approximate constant of the motion. Finally, at long times, all trajectories are attracted to a one-dimensional manifold as the constant of motion is lost. The general structure of the attracting manifolds remains qualitatively similar at other temperatures, pressures, and fuel mixtures. Of course the quantitative details of the manifolds evolve as these parameters are varied.

The manifolds are explicitly constructed in Figure 4 for the case of $T = 2000$ K, $p = 0.276$ bar, $C_1 = 10^{16}/\text{cm}^3$, and $C_2 = 1.5 \times 10^{16}/\text{cm}^3$. The one-dimensional manifold, M_1, is plotted with a solid line extending from the boundary of the physical phase space (i.e., positive concentrations). The two-dimensional manifold, M_2, is depicted with a set of rulings. The rulings of a two-dimensional manifold emanate from M_1 and are curves along which N is roughly conserved. Trajectories are plotted which attract first to the two-dimensional manifold, and then to the one-dimensional manifold. It is clear that the approach to equilibrium follows a cascade of manifolds of lowering dimension.

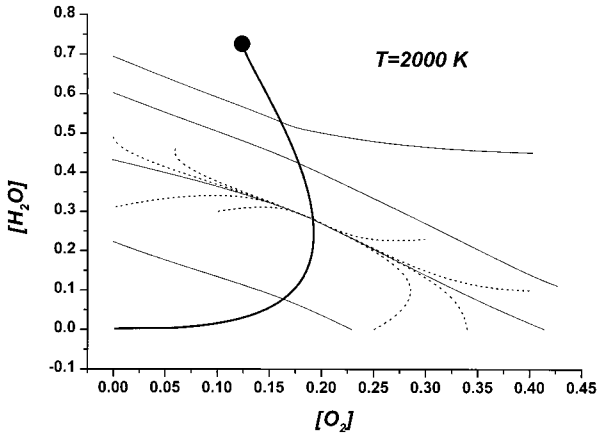

Figure 4. One- and two-dimensional ALDM for the hydrogen combustion model obtained using the global eigenvalue method. The system parameters were chosen to be $T = 2000$ K, $p = 0.207$ bar, $C_1 = 10^{16}/\text{cm}^3$, and $C_2 = 1.5 \times 10^{16}/\text{cm}^3$. The bold line is the one-dimensional manifold, whereas the solid lines are the rulings of the two-dimensional manifold. The dashed lines are selected trajectories that show sequential attraction to the two- then one- dimensional manifold.

On a physical level, the reason for the occurrence of the approximate constant of motion, N, is the existence of a reduced kinetic scheme that is accurate on intermediate time scales. Traditional kinetic analysis has identified the subsystem of reactions consisting of steps 1−8 from Table 1 as an accurate reduced mechanism on intermediate times.[26,27] All these reactions are of the form $X + Y \rightarrow W + Z$, i.e., chain propagating steps, which clearly conserve the total number of molecules. On long time scales, the slower reactions from Table 1 begin to contribute and break the constant of motion.

A few more remarks should be made about the construction of the manifolds in Figure 4. The manifolds were obtained using the global eigenvalue method discussed in the previous section. The essential strategy in constructing the two-dimensional manifold, M_2, is to begin by computing the one-dimensional manifold, M_1. To achieve this, we hold $[O_2]$ fixed at 0, which is the boundary of the physical phase space, to select initial conditions. Then trajectories were propagated backward for times up to 10^{-3} sec. The fastest *N-1* eigenvectors of **M** were forced to have zero components along the flow using a Newton-search for a root in initial condition space. The full manifold M_1 is then found by propagating the root initial condition until equilibrium is reached. Next, starting from initial conditions on a hyperplane far from M_1, defined by $y_k = \text{const}$, trajectories are propagated forward until they reach the close vicinity of M_1, $Min_s|\mathbf{y}(t) - \mathbf{Y}(s)| < \epsilon$ then backward to test their stability. For a given ruling, a particular value $s = s_0$ is selected, which defines the point at which the ruling curve connects to M_1 within a tolerance ϵ. Holding y_k and s_0 fixed, the *N-2* fastest eigenvectors of **M** are forced to zero using a Newton-search in the initial condition space. Each point on M_1 is the termination of two rulings on M_2, which are roughly curves of constant N in the phase space. Each of these ruling is the attracting curve for a family of trajectories with the same value of N on the intermediate time scale.

We have also applied the other techniques described in section II to the construction of manifolds for this problem. The Maas−Pope algorithm was found to provide a very accurate approximation for M_1, often better than three figure precision. Significant errors were only seen for extreme choices of system parameters. However, we found the Maas−Pope algorithm was difficult to apply for the two-dimensional manifold due to

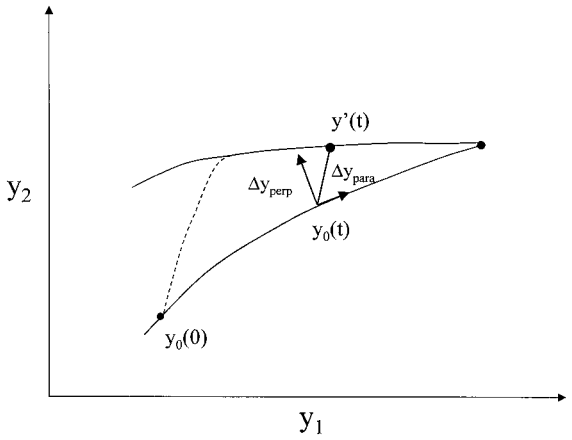

Figure 5. Schematic view of the sensitivity of a one-dimensional ALDM. The unperturbed manifold is labeled by $\boldsymbol{y}_0$, whereas the perturbed manifold is labeled by $\boldsymbol{y}'$. A perturbed trajectory is shown to develop a perpendicular and a parallel component of displacement.

numerical instability. It is likely that more sophisticated extrapolation techniques such as described in ref 13 are required to obtain M_2 for this system. The predictor−corrector method converges robustly to the result obtained using the global eigenvalue method for M_1. The predictor−corrector has not yet been extended to higher-dimensional manifolds. The modified Fraser's algorithm also gives essentially exact results for the one-dimensional manifold. Using a steady-state approximation to M_1 as the initial guess, the algorithm converges within 10 iterations. However, due to the stiffness of the problem, each iteration needed to be broken into about 100 integration steps to ensure stability. We could not provide a satisfactory initial guess for the modified Fraser algorithm to locate the two-dimensional manifold, although not a great deal of effort was expended in testing various possibilities.

As an example of the use of the manifold concept in practical kinetics, consider the application of the ALDM for chemical sensitivity analysis. Sensitivity analysis is widely employed to study the importance of specific reactions or species on the overall reaction kinetics. In conventional sensitivity analysis, a trajectory is started at a useful initial condition and the sensitivity of the concentrations is measured at a later time when, e.g., certain rate constants are altered. The basic unit of description is the sensitivity matrix

$$S_{i,j}(t) = \frac{\partial y_i(\boldsymbol{y}_0,t;\mathbf{k})}{\partial k_j} \tag{3.2}$$

where k_j are the sensitivity parameters (e.g., the rate constants). In the conventional treatment, the sensitivity of "final" concentration will have contributions from both the transient kinetics and the asymptotic manifold kinetics.

We formulate the problem in a somewhat different fashion by considering the sensitivity of the ALDM itself to perturbations in the mechanism. In this way, the sensitivity of the reduced mechanism to perturbation is measured. Thus, for a one-dimensional manifold, we imagine the parametrization

$$\mathbf{Y}(s,\mathbf{k}) = [y_1(s,\mathbf{k}), y_N(s,\mathbf{k})]^T \tag{3.3}$$

where $\boldsymbol{k}$ represent, e.g., rate constants. The sensitivity of the kinetics to $\boldsymbol{k}$ can be decomposed into two parts: the (perpendicular) displacement of the manifold in phase space, and the perturbation of a trajectory along (parallel) the manifold. As illustrated in Figure 5, a trajectory started at a point on the unperturbed manifold will quickly attract to the perturbed manifold, thus developing a perpendicular component of displacement independent of starting point (but depending on s, the final point), and a parallel component depending on both initial and final conditions. The two sensitivities have different physical meanings. The perpendicular sensitivity represents change in the actual reduced mechanism, whereas the parallel sensitivity reflects an overall rescaling of time within the same reduced mechanism. The logarithmic sensitivities to changes in the i^{th} rate constant, k_i, can be measured using

$$G_i^{\perp}(s,\mathbf{k}) = \sqrt{\sum_j \left[\frac{\mathrm{d}\ln(\Delta Y_j^{\perp}(s,\mathbf{k}))}{\mathrm{d}\ln(k_i)}\right]^2} \tag{3.4}$$

and

$$G_i^{||}(s,\mathbf{k}) = \sqrt{\sum_j \left[\frac{\mathrm{d}\ln(\Delta Y_j^{||}(s,\mathbf{k}))}{\mathrm{d}\ln(k_i)}\right]^2} \tag{3.5}$$

The displacements $\Delta Y_j^{||}$ and $\Delta Y_j^{\perp}$ are between the unperturbed trajectory $\boldsymbol{y}_0$, and the perturbed trajectory $\boldsymbol{y}'$, originated at the same initial phase space point (on the unperturbed manifold) and propagated for equal times. Here, s is the parametrization along the unperturbed manifold. The displacements may be computed by using satellite trajectories, or by using the expression for linearized dynamics in the perturbation Δk_i

$$\Delta\mathbf{y}(t) = \int_0^t \mathbf{M}(t,t') \cdot \frac{\partial \mathbf{f}(\boldsymbol{y}_0)}{\partial k_i}\Delta k_i dt' + \mathbf{M}(t,0)\cdot\Delta\mathbf{y}(0) \tag{3.6}$$

The matrix $\mathbf{M}$ is for unperturbed motion and, in the present case, the initial displacement of the orbit, $\Delta\boldsymbol{y}(0)$, is zero.

In Figure 6, the sensitivity of the kinetics is plotted for the case $T = 1500$ K, $p = 0.207$ bar, $C_1 = 10^{16}/\mathrm{cm}^3$, and $C_2 = 1.5 \times 10^{16}/\mathrm{cm}^3$. The reaction index labels the reactions using the numbering scheme shown in Table 1. The manifold is parametrized using the logarithm of time. In the upper panel, the conventional sensitivity is shown. In the lower two panels, the parallel and perpendicular components are displayed. It is clear that the position of the manifold, reflected in the perpendicular sensitivity, is dominantly determined by the first 8 reactions. This is consistent with the reduced mechanism of Michael that was deduced using standard kinetics. Reaction 12, formation of the peroxy-radical, also has a minor effect on the location of the manifold. Moreover, we see that the forward and backward reactions of the subsystem 1−8 are nearly in equilibrium, so that, e.g., the sensitivity of reaction 1 is nearly equal to that of reaction 2, etc. Thus, the position of the one-dimensional manifold may be found to good accuracy simply by determining the equilibrium points of the subsystem 1−8 over the full range of values for the total concentration, N.

The parallel sensitivities are dramatically different from the perpendicular components. Reactions 9 (hydrogen recombination) and 12 (peroxy-radical formation) show the most sensitivity for much of the manifold. These reactions mediate a decrease in the total concentration, thus breaking the approximate conservation of N that govern the subsystem 1−8 kinetics. The parallel sensitivities thus reflect the dominant reactions for breaking the conservation of N. As the manifold approaches equilibrium at long times, we also see reactions 24 (OH-recombination) and 38 (peroxide decomposition) coming in with nearly equal sensitivities, again with near microreversibility.

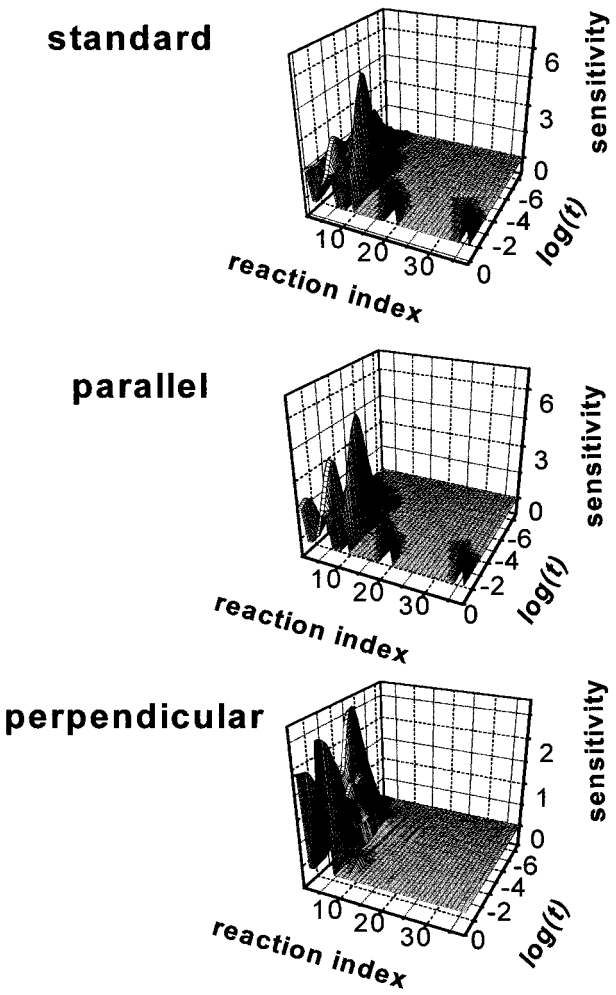

Figure 6. Logarithmic sensitivity of kinetic trajectories plotted vs reaction index, see Table 1, and the manifold parametrization $s = \log(t)$. The conditions chosen for the simulation are $T = 1500$ K, $p = 0.276$ bar, $C_1 = 10^{16}/\text{cm}^3$, and $C_2 = 1.5 \times 10^{16}/\text{cm}^3$. The upper panel shows the conventional sensitivity. The lower panels depict the perpendicular and parallel sensitivities.

The conventional sensitivity, shown in the upper panel of Figure 6, does not distinguish parallel, perpendicular, or transient sensitivity. At very early times, $t < 10^{-4}$ sec, the standard result resembles neither the parallel or perpendicular components and reflect only transient dynamics. At longer times, the standard sensitivity most strongly reflects the parallel manifold sensitivity. Thus, in a sense, the standard sensitivity is more of a measure of the rate of approach to equilibrium (i.e., a time-rescaling) than it is an indicator of the appropriate subsystem that determines the phase space position of the ALDM.

IV. Conclusions

The use of ALDM's provides a natural approach to simplify complicated systems of kinetics equations. On long time scales, kinetics trajectories automatically seek out common pathways to approach equilibrium. If the appropriate ALDM can be constructed explicitly, the kinetic rate equations can be written and solved in a much lower dimensional representation. The practical advantages of such a reduction scheme are clear because huge computational savings may accrue. The conceptual advantages of using ALDM are equally important and derive from adopting a geometrical viewpoint of the manifold. The position of the ALDM in phase space provides a transparent means to assess the relative importance of various reactions and species in the overall mechanism. The dimensionality of the manifold provides an indication of the minimum number of independent species required to simulate the kinetics on a given time scale; and the change in the manifold dimension as time scale increases probes the cascade of reduced mechanisms.

In this article, we have presented a general discussion of a number of techniques for the construction of ALDM's, and discussed their relative advantages. The modified Fraser algorithm was presented in more detail than in our previous work. Most importantly, a new method, the global eigenvalue method, was presented here for the first time. This method was shown to be a natural extension of the MP-method to global trajectory dynamics. This method has the important advantage over other trajectory-based methods in that higher dimensional ALDMs can be generally constructed. Because the length of time propagation is a convergence parameter, the MP-method can be regarded as the $\Delta t \rightarrow 0$ limit of this more general technique. The application of the global eigenvalue method to the hydrogen combustion problem demonstrated that the method works well when applied to realistic kinetics problems. Finally, it was shown that sensitivity analysis could be formulated in a more useful way when combined with the ALDM. The sensitivity of the position of the ALDM with respect to changes in rate constants provides a means to assess the sensitivity of the reduced mechanism itself. Conventional sensitivity analysis does not distinguish between sensitivity of the transient, for which no reduced model may exist, and that of the long time asymptotic behavior.

Acknowledgment. R.T.S. was supported by a grant from the National Science Foundation and the visiting scientist program at Argonne National Laboratory, and M.J.D. was supported by the Office of Basic Energy Sciences, Division of Chemical Sciences, U.S. Department of Energy, under Contract No. W-31-109-ENG-38. We are grateful to J. Michael and J. Hessler for useful conversations.

References and Notes

(1) Pilling, M. J.; Seakins, P. W. *Reaction Kinetics*; Oxford University Press: Oxford, 1995.
(2) Chevalier, C.; Pitz, W. J.; Warnatz, J.; Westbrook, C. K.; Melenk, H. *24th International Symposium on Combusion:* Combustion Institute: Pittsburgh, 1992; p 93.
(3) Shampine, L. S. *Numerical Solution of Ordinary Differential Equations*; Chapman & Hall: New York, 1994.
(4) Hindmarch, A. C. In *Scientific Computing*; Stepleman, R. S. Ed.; North-Holland: Amsterdam, 1983; p 55.
(5) Warnatz, J.; Maas, U.; Dibble, R. W. *Combustion*, Springer: Berlin, 1996.
(6) Okino, M. S.; Mavrovouniotis, M. L. *Chem. Rev.* **1998**, *98*, 391, and references therein.
(7) Tomlin, A. S.; Turanyi, T.; Pilling, M. J. *Comput. Rev. Chem. Kinetics* **1997**, *35*, 293, and references therein.
(8) Tomlin, A. S.; Turanyi, T.; Pilling, M. J. *J. Phys. Chem.* **1993**, *97*, 163.
(9) Li, G.; Rabitz, H.; Toth, H. *Chem. Eng. Sci.* **1994**, *49*, 343; Li, G.; Rabitz, H.; Toth, H. *Chem. Eng. Sci.* **1991**, *46*, 95.
(10) Lam, S. H.; Goussis, D. A. *Int. J. Chem. Kinet.* **1994**, *26*, 461.
(11) Maas, U.; Pope, S. B. *Combust. Flame* **1992**, *88*, 239.
(12) Maas, U.; Pope, S. B. *24th International Symposium on Combusion*; Combustion Institute: Pittsburgh, 1992; p 102; Maas, U.; Pope, S. B. *25th International Symposium on Combusion*, Combustion Institute: Pittsburgh, 1994; p 1349.
(13) Maas, U. *Appl. Math.* **1995**, *3*, 249.
(14) Schmidt, D.; Blasenberg, T.; Maas, U. *Combust. Theory Modeling* **1998**, *2*, 135.
(15) Davis, M. J.; Skodje, R. T. *J. Chem. Phys.* **1999**, *111*, 859.
(16) Davis, M. J.; Skodje, R. T. *Z. Phys. Chem.* **2001**, *215*, 233.
(17) Fraser, S. J. *J. Chem. Phys.* **1988**, *88*, 4732.
(18) Roussel, M. R.; Fraser, S. J. *J. Chem. Phys.* **1990**, *93*, 1072.
(19) Nguyen, A. H.; Fraser, S. J. *J. Chem. Phys.* **1989**, *91*, 186.

(20) Roussel, M. R.; Fraser, S. J. *J. Phys. Chem*. **1991**, *95*, 8762.
(21) Schutz, B. *Geometrical Methods of Mathematical Physics*; Cambridge University Press: Cambridge, 1980.
(22) Roussel, M. R., Ph.D. Thesis, University of Toronto, 1994.
(23) Arnold, V. I. *Geometric Methods in the Theory of Ordinary Differential Equations*; Springer-Verlag: Berlin, 1983.
(24) Pechukas, P.; Light, J. C. *J. Chem. Phys*. **1966**, *44*, 3897.
(25) Bjorken, J. D.; Drell, S. D. *Relativistic Quantum Mechanics*; McGraw-Hill: New York, 1964.
(26) Michael, J. V. Prog. *Energy Combust. Sci*. **1992**, *18*, 327.
(27) Su, M.-C.; Kumaran, S. S.; Lin, K. P.; Michael, J. V. *Rev. Sci. Instrum.* **1995**, *66*, 4649.